

# bradscholars

## Solid-State Competitive Destabilization of Caffeine Malonic Acid cocrystal: Mechanistic and Kinetic Investigation

Item Type	Article
Authors	Alsirawan, M.B.;Lai, X.;Prohens, R.;Vangala, Venu R.;Pagire, Sudhir K.;Petroc, S.;Bannan, T.J.;Topping, D.O.;Paradkar, Anant R
Citation	Alsirawan MB, Lai X, Prohens R et al (2020) Solid-State Competitive Destabilization of Caffeine Malonic Acid cocrystal: Mechanistic and Kinetic Investigation. <i>Crystal Growth and Design</i> . 20(12): 7598-7605.
DOI	<a href="https://doi.org/10.1021/acs.cgd.0c01246">https://doi.org/10.1021/acs.cgd.0c01246</a>
Publisher	American Chemical Society
Rights	(c) 2020 ACS. Full-text reproduced in accordance with the publisher's self-archiving policy.
Download date	2025-06-17 04:24:01
Link to Item	<a href="http://hdl.handle.net/10454/18305">http://hdl.handle.net/10454/18305</a>

# Solid-State Competitive Destabilization of Caffeine Malonic Acid Cocrystal: Mechanistic and Kinetic Investigations

*MHD. Bashir Alsirawan,<sup>\*a</sup> Xiaojun Lai,<sup>b</sup> Rafel Prohens,<sup>c</sup> Sudhir K Pagire, Venu R. Vangala,<sup>a</sup> Petroc Shelley,<sup>d</sup> Thomas J. Bannan,<sup>e</sup> David O. Topping,<sup>d,e</sup> and Anant Paradkar<sup>\*a</sup>*

a. Centre for Pharmaceutical Engineering Science, University of Bradford, Bradford, D7 1DP, United Kingdom.

b. School of Chemical and Process Engineering, University of Leeds, Leeds, LS2 9JT, United Kingdom.

c. Polymorphism and Calorimetry Unit, University of Barcelona, Lluís Solé i Sabarís, 08028 Barcelona, Spain.

d. School of Earth and Environmental Sciences, University of Manchester, Manchester, M13 9PL, United Kingdom.

e. National Centre for Atmospheric Science, University of Manchester, Manchester, M13 9PL, United Kingdom.

## **ABSTRACT:**

The main objective of this research is to investigate both mechanism and kinetics of solvent free destabilization of the model caffeine : malonic acid cocrystal (CA:MO 2:1) in presence of oxalic acid (OX) as a structural competitor to malonic acid (MO). Competitive destabilization of CA:MO and subsequent formation of caffeine : oxalic acid (CA:OX) takes place at temperatures significantly below their melting points. Destabilization mechanism was found to be mediated by sublimation of both CA:MO and OX. During CA:MO destabilization, free CA could not be detected and direct transformation to CA:OX cocrystal was observed. The destabilization kinetics follow Prout-Tompkins nucleation and crystal growth model with activation energy of 133.91 kJ/mol and subsequent CA:OX growth kinetics follow Ginstling – Brounshtien and 3D diffusion models with activation energy range of 130.45 - 132.57 kJ/mol.

## INTRODUCTION

Tracking of chemical reactions that occurs in industry during processing or storage stage is crucial to understand their nature, which enable controlling them to get the optimum outcome.<sup>1</sup> Among these reactions cocrystallization has proven a great potential to improve the development of pharmaceutical, nutritional, agricultural, and energetic materials.<sup>2-4</sup> Cocrystals are obtained from the interaction of two or more solid compounds via intermolecular forces such as hydrogen bonding and aromatic interactions.<sup>5</sup> The complexity of handling cocrystals stems from their multicomponent nature which must be preserved during all processing stages. However, cocrystal lattice can destabilize in many ways including dissociation, solvation, polymorphic transformation, and stoichiometric changes. Moreover, these changes can occur under a variety of processing conditions like temperature, humidity, etc. Additionally, the use of additives during processing is common in the industry and many of them have been found to be further interfering with cocrystals, thus complicating their stability.<sup>6</sup> One of such interferences involving the additive competing with one of the cocrystal structural component leading to its replacement by that additive.<sup>7,8</sup> Understanding competitive destabilization of cocrystals offers crucial information to obtain a robust cocrystal manufacturing process with common additives or excipients.

Competitive destabilization pathway of two carbamazepine cocrystals at solvent free conditions was found to vary depending on the sublimation/melting behavior of the components as well as on the processing conditions.<sup>9</sup> Carbamazepine : nicotinamide 1:1 cocrystal (CZ:NT) can destabilize in presence of saccharin (SA) at relatively high temperatures via eutectic phase resulting in the formation of carbamazepine : saccharin 1:1 cocrystal (CZ:SA). On the other hand, presence of NT with CZ:SA during neat grinding or at lower temperatures causes the destabilization of CZ:SA via vapor phase and results in the formation of CZ:NT. Thermodynamic calculations associated with previous observations show that eutectic mediated transformation of CZ:NT to CZ:SA can be predicted by fusion enthalpy differences. Whereas, vapor mediated transformation of CZ:SA to CZ:NT is driven by vapor pressure differences of components and can be predicted by Gibbs free energy difference of sublimation.

Previous report showed that solvent free formation of CA:MO or CA:OX cocrystal occurs when the pure coformer MO or OX reaches enough vapor pressure which enables interacting with CA.<sup>10</sup> Additionally, solvent free grinding of CA:MO 2:1 in presence of OX causes destabilization of the cocrystal and subsequent formation of CA:OX 2:1.<sup>8</sup> These observations

suggest that competitive destabilization of CA:MO cocrystal is likewise mediated by vapor phase formation.

This paper aims to further investigate the mechanism of CA:MO destabilization in presence of OX at solvent free conditions and it reports for the first time *in-situ* monitoring of the reaction using Raman microscopy and variable temperature powder X-ray diffraction (VT\_PXRD). Thermal analysis using differential scanning calorimetry (DSC) and thermogravimetric analysis (TGA) was conducted as an initial investigation and to observe thermal behavior of the cocrystals, their components, and physical mixtures. Then, solvent free competitive destabilization experiments were conducted using only heat by VT\_PXRD. Sublimation apparatus was utilized to identify sublimation outcomes of all cocrystals, and related components and structural investigation of sublimates and residuals was conducted using PXRD and Raman analysis. Computational calculations of lattice energies and vapor pressure measurements were performed for all components. Moreover, the reaction was monitored at four predetermined temperatures. Subsequently, mechanistic model fitting was performed, and activation energy was calculated using Arrhenius equation. Additional tracking of destabilization reaction was carried out visually using hot-stage microscopy to provide further insights into the process (all method details are available in the Supporting Information, SI).

Thermal analysis thermograms are present and summarized in the SI (Figures S4 – S8, and Table S2). TGA results showed significant weight loss (ca. 24.7%) from CA:MO cocrystal consistent with the theoretical content of MO (ca. 21.1%) starting at 122.1 °C below CA:MO melting point (132.1 °C). Similarly, CA:OX exhibits (8.5%) weight loss starting from 86.0 °C and significantly below its melting point (208.7 °C). It was confirmed using heat-cool-heat that it is not a desolvation event. Moreover, the loss on weight is below theoretical content of OX in the cocrystal (18.8%). Additionally, CA displays a weight loss at 167.2 °C above its phase transition of  $\beta$  to  $\alpha$  form at 144.5 °C and significantly lower than the melting point of its  $\alpha$  form (235.93 °C).<sup>11</sup> Likewise, pure OX and MO show weight losses at 120.4 and 129.8 °C below their melting points at 189.1 and 130.66 °C, respectively. TGA results indicate a potential sublimation of CA:MO, and CA:OX with sublimation of pure  $\alpha$ -CA, MO, and OX being previously reported<sup>12</sup>. DSC thermograms of the physical mixtures (PM) of 2:1 CA+MO and CA+OX exhibit three endotherms. For CA+MO PM, the endotherms are at 96.1, 130.8, and 236.1 °C related to eutectic formation, CA:MO cocrystal melting, and CA melting, respectively. In case of CA+OX PM, the endotherms were found at 115.7, 206.4, and 234.2 °C also related to eutectic formation, CA:OX cocrystal melting, and subsequent CA melting,

respectively. DSC Thermogram of CA:MO + OX shows an endotherm at 92.8 °C coincident with a weight loss onset of 104.62 °C observed by TGA. This event is suggested to be a sublimation event where destabilization of CA:MO and formation CA:OX occur. Moreover, the thermogram shows endotherm at 131.51 °C which can be assigned to the melting of unreacted CA:MO or MO after being replaced with OX. Two additional endotherms were observed at 208.05 and 234.86 °C related to melting of formed CA:OX and CA, respectively.

PXRD results show that transformation of stoichiometric CA:MO + OX mixture to CA:OX started at 60 °C and was completed at 100 °C (Figure 1). Pure CA peaks were not observed during the transformation, and transformation occurred below both melting point of CA:MO (132.1°C) and eutectic point of CA + MO (96.1 °C). Additional VT-PXRD experiment was conducted on pure CA:MO to check its integrity at elevated temperatures, and no dissociation was observed even at 100 °C. This confirms that destabilization of CA:MO + OX is not mediated by CA:MO melting and presence of OX triggered the reaction at much lower temperatures.

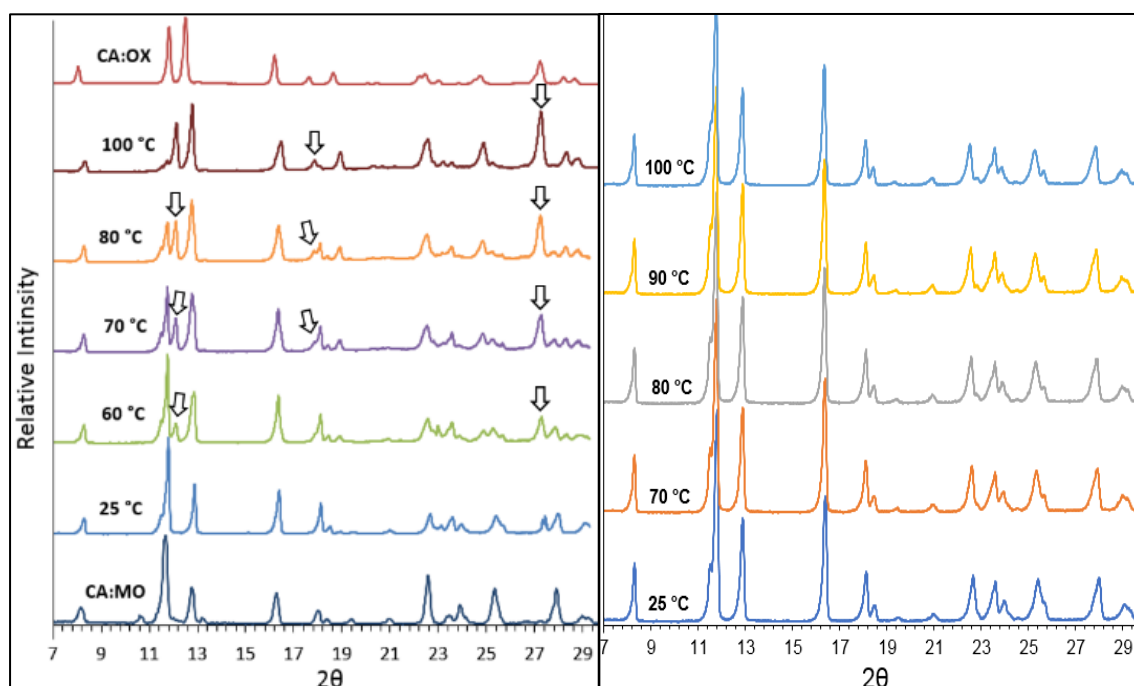


**Figure 1.** PXRD patterns from bottom to top; (Left): Experimental CA:MO cocrystal, CA:MO + OX at 25 through 100 °C, and experimental CA:OX cocrystal. (Right): CA:MO cocrystal maintained isothermally at 25 through 100 °C.

Moreover, according to thermal analysis, CA:MO undergoes weight loss before reaching the melting point. Therefore, we hypothesize that competitive destabilization of CA:MO by OX occurs at the vapor phase (Figure 2).

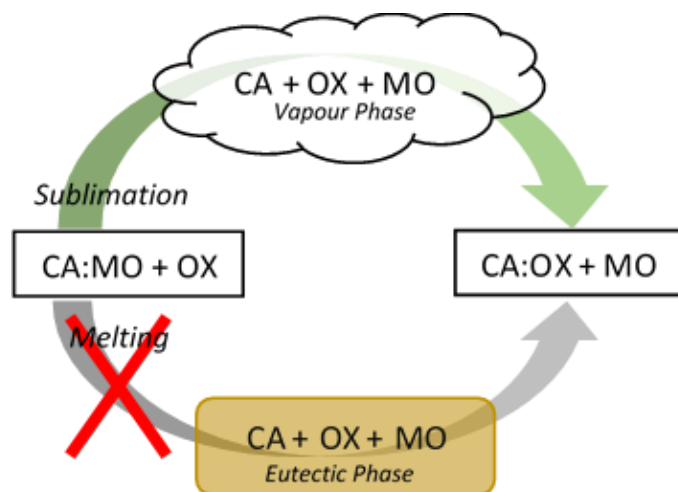


**Figure 2.** Proposed mechanism for competitive destabilization of CA cocrystals induced by solvent free processing.

To further understand vapor phase mediated destabilization of CA:MO, sublimation experiments were carried out using sublimation apparatus. The experiment is conducted by placing ca. 1 g of sample into sublimation reservoir then heated to a predetermined temperature. Subsequently, sublimates on top and residuals at bottom were collected and analyzed by PXRD, and Raman spectroscopy (SI, Figures S9 and S10). Two temperatures were considered for CA system, 90 and 120 °C, which are below and above endotherm and weight loss points (ca. 104 °C) of CA:MO+OX. The results suggest that pure CA and MO display sublimation only at 120 °C and the  $\alpha$  form of CA is eventually obtained (SI, Table S3). In addition, OX show high sublimation at 90 and 120 °C. However, it is obtained in the form of dihydrate (OX DH), which is due to water uptake from atmosphere as all starting materials were previously confirmed to be anhydrous. Pure CA:MO exhibited sublimation only at 120 °C showing  $\alpha$ -CA at both top and bottom, while no sublimation or structural change was observed at 90 °C. CA:OX did not exhibit any sublimation at 90 or 120 °C. (CA+OX+MO) PM and CA:MO + OX show OX DH as sublimate and CA:OX formed on the bottom. CA:MO and OX were also placed in sublimation chamber with physical barrier which prevent any contact between the two. After 24 hours no reaction was observed at 90 °C. However, at 120 °C CA:OX appeared on both sides indicating that destabilization of CA:MO and formation of CA:OX took place via sublimation of both CA:MO and OX. This is consistent with the thermograms showing sublimation peak and weight loss at ca. 103 °C. Moreover, competitive destabilization can take place far below that temperature provided CA:MO is in contact with OX.

Visualization during destabilization reaction of CA:MO in presence of OX showed sublimation of OX at 80 °C followed by formation of new crystals taking place at vapor zones. These crystals were matched to CA:OX crystals (Figure 3). CA:OX crystals kept growing even after reaching 120 °C (Figure 4). Crystal assignment was performed using Raman microscopy.

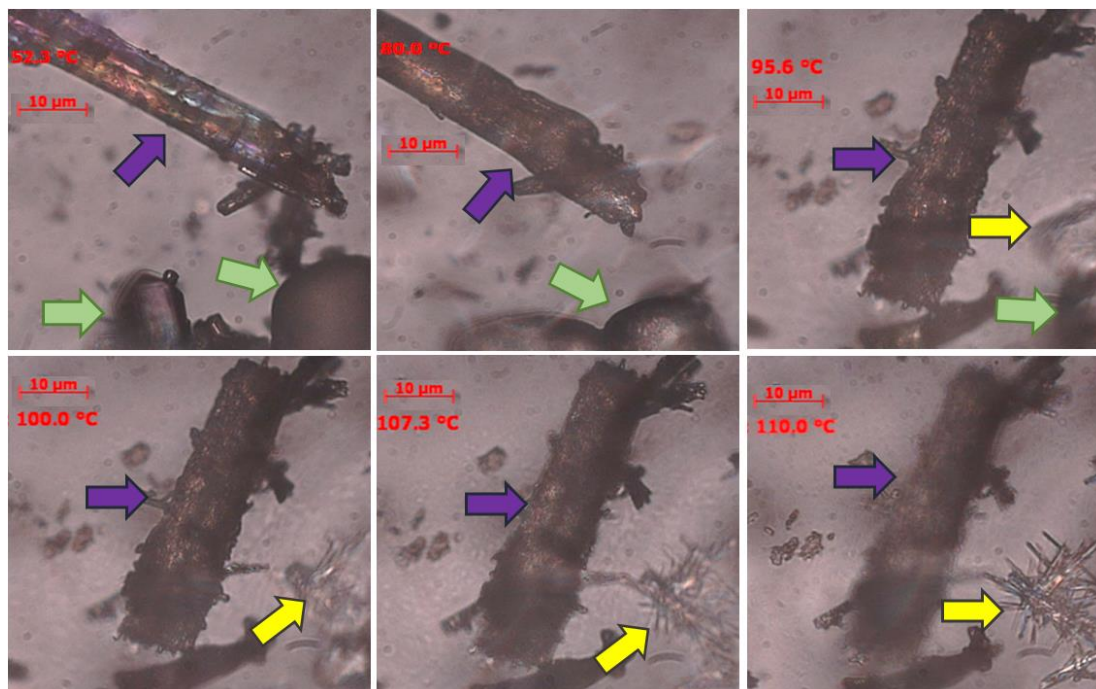


**Figure 3.** HSM images of CA:MO destabilization in presence of OX and formation of CA:OX. Purple arrows indicate CA:MO, yellow arrows: CA:OX, and green arrows: OX.

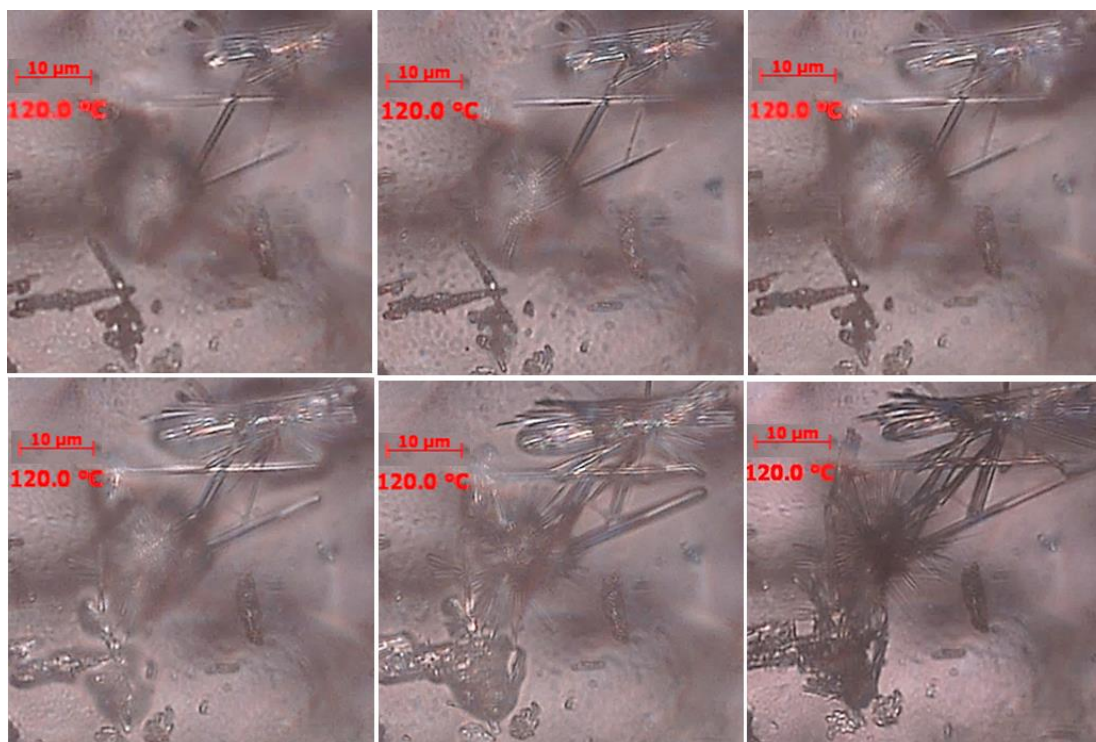


**Figure 4.** Crystal growth of CA:OX during destabilization of CA:MO in presence of OX.

In order to understand experimental observations, energy calculations were conducted and correlated with that of experimental results. As previously reported, destabilization reaction involves reaching equilibrium phase either as vapor or eutectic phase as in case of previously reported CZ:NT destabilization.<sup>9</sup> This is followed by the formation of the thermodynamic preferred cocrystal (Equation 1).



Thermodynamic parameters including fusion enthalpies, saturated vapor pressures and lattice energies were used for the energy calculations. Lattice energies were calculated previously using Density Functional Theory (DFT)<sup>8</sup>, and fusion enthalpies were determined using DSC (Table 1). Whereas, vapor pressures were measured at a range of temperatures (298 to 328K) using Knudsen Effusion Mass Spectrometry (KEMS).<sup>13</sup> Details of these methods can be found in the SI.

**Table 1.** Lattice Energies ( $E$ ) of CA:MO, CA:OX and Pure Components Calculated using DFT and Fusion Enthalpies ( $\Delta H_{\text{fus}}$ ):

Name	$E^*$ kJ/mol	$\Delta H_{\text{fus}}$ kJ/mol
CA	-15.29	19.27
MO	-6.86	23.30
OX	-5.21	58.52
CA:MO	-35.83	15.90
CA:OX	-37.45	31.05

\* Reported values.<sup>8</sup>

Subsequently, energy calculations of destabilization were conducted based on (Equation 1). Lattice energy difference of destabilization ( $\Delta E_{\text{des}}$ ) (Equation 2), Fusion enthalpy of destabilization ( $\Delta H_{\text{fus-des}}$ ) (Equation 3) and sublimation Gibbs free energy ( $\Delta G_{\text{sub-des}}$ ) (Equation 4) were calculated.

$$\Delta E_{\text{des}} = E(\text{CA:OX}) + E(\text{MO}) - [E(\text{CA:MO}) + E(\text{OX})] \text{ (Eq2)}$$

$$\Delta H_{\text{fus-des}} = H_{\text{fus}}(\text{CA:OX}) + H_{\text{fus}}(\text{MO}) - [H_{\text{fus}}(\text{CA:MO}) + H_{\text{fus}}(\text{OX})] \text{ (Eq3)}$$

$$\Delta G_{sub-des}^{\circ} = -RT \ln \frac{P_{CA:MO} P_{OX}}{P_{CA:OX} P_{MO}} \quad (\text{Eq4})$$

Where  $R$ ,  $T$ ,  $P$  values are gas constant, absolute temperature and vapor pressure, respectively.  $\Delta E_{des}$  (-24.23 kJ/mol) and  $\Delta H_{fus-des}$  (-20.08 kJ/mol) show that CA:OX is thermodynamically favorable (Table 2). Moreover,  $\Delta G_{sub}$  at all tested temperatures gave negative values (Table 3) indicating that vapor mediated reaction favors CA:OX formation confirming experimental findings.

**Table 2.** Destabilization Related Lattice Energy Change ( $\Delta E_{des}$ ), Fusion Enthalpy Change ( $\Delta H_{fus-des}$ ), and Sublimation Gibbs Energy Change ( $\Delta G_{sub-des}$ ) Linked to Observed Cocrystal (Equation 1) as a result of Neat Grinding (NG) and Heat.

$\Delta E_{rep}$	$\Delta H_{fus-des}$	$\Delta G_{sub-des}$ 298K	Process	Observed
-24.23 kJ/mol	-20.08 kJ/mol	-8.81 kJ/mol	NG	CA:OX
			Heat	CA:OX

**Table 3:** Sublimation Gibbs Free Energy Changes using Measured Vapor Pressure Values ( $P$ ) at Temperature Range of 298 – 328 K.

$T(K)$	$\Delta G_{sub}$ (J/mol)	$P_{CA:MO}$	$P_{CA:OX}$	$P_{OX}$	$P_{MO}$
298	-8808.996	0.00109	0.00147	0.0095	0.00020
303	-8501.609	0.00131	0.00189	0.0157	0.00037
308	-7828.283	0.00197	0.00350	0.0255	0.00067
313	-6480.510	0.00245	0.00690	0.0407	0.00120
318	-4794.884	0.00368	0.01840	0.0640	0.00209
323	-4302.917	0.00719	0.04020	0.0993	0.00358
328	-4339.030	0.01270	0.06520	0.1521	0.00603

The experimental observations along with thermodynamic calculations reflect that competitive destabilization of CA:MO and its transformation to CA:OX is restricted to vapor phase pathway and no eutectic is reached or observed. On the other hand, CZ:NT transforms to CZ:SA in presence of SA via eutectic phase which is governed by the lattice energy and fusion enthalpy difference. Whereas, transformation of CZ:SA to CZ:NT in presence of NT occurs only via vapor formation and is governed by Gibbs free energy of sublimation (Figure 10).

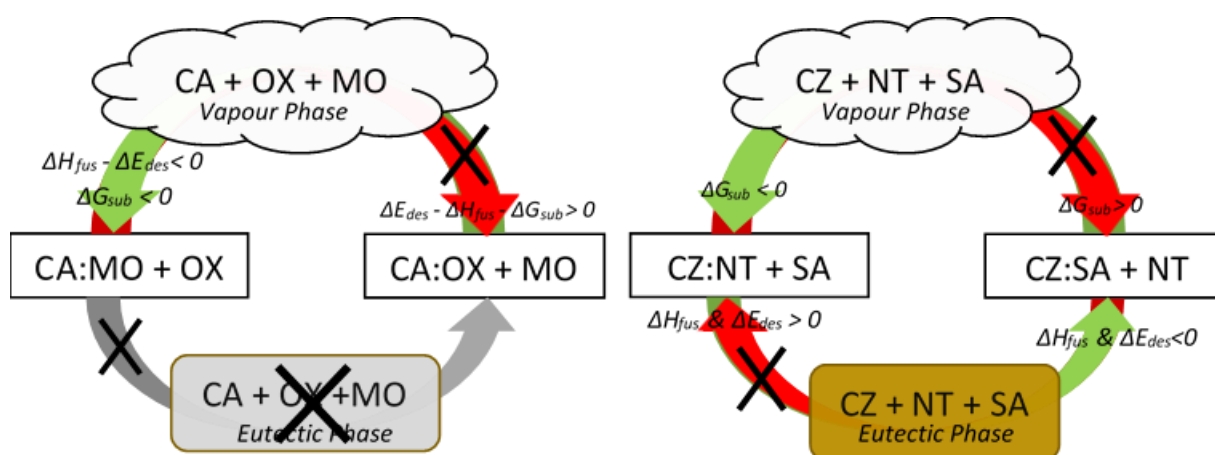


**Figure 5:** Schematic representation of eutectic or vapor phase mediated competitive destabilization of CA (Left) and CZ<sup>9</sup> (Right) cocrystals.

*In-situ* monitoring of Raman spectra show gradual decrease of CA:MO peaks at 790, 910, 1330, and 1415  $\text{cm}^{-1}$  after 2 minutes. Subsequently, peaks of CA:OX appeared at 840, 890, 1310, and 1405  $\text{cm}^{-1}$  (Figure 6).

*In-situ* tracking using VT\_PXRD at 70 °C (Figure 7) was performed at four isothermal conditions, 70, 80, 90 and 100 °C. While tracking the reaction at 70 °C, PXRD patterns showed gradual reduction of CA:MO peaks at 8.1, 11.64, 12.72, 16.25, 22.6, 23.92, 25.34, 27.96, 31.32, and 32.2° 2 $\theta$  together with reduction of OX peaks at 22.92, 27.22, 30.98, 31.52, 33.08, 37.38, and 38.74° 2 $\theta$ . This was followed by appearance of CA:OX peaks at 8.18, 11.98, 12.68, 16.42, 18.86, 22.84, 25.14, 27.7, 28.58, and 31.12° 2 $\theta$ . VT\_PXRD kinetics for reactions at 80, 90, and 100 C can be found in SI (Figures S11-S13).

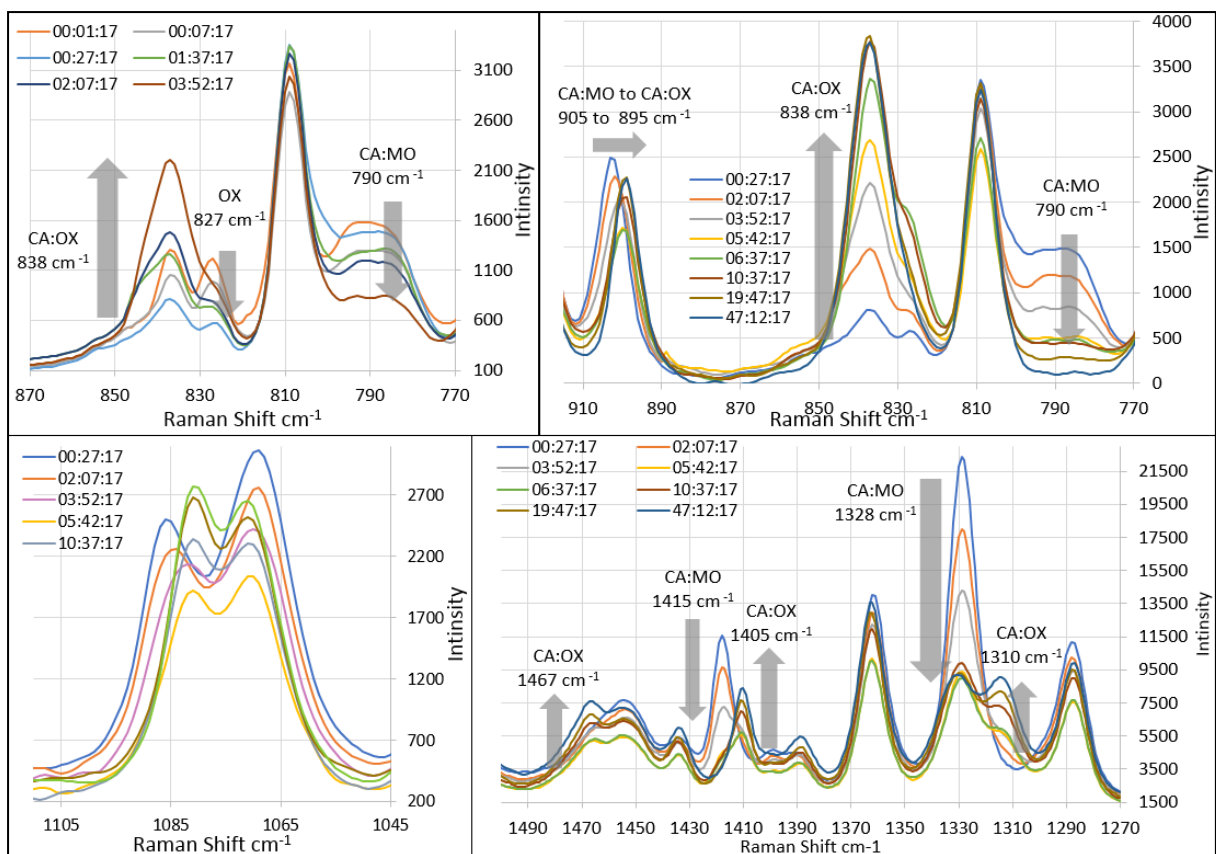


**Figure 6.** *In-situ* Raman spectra of CA:MO + OX at 70 °C showing appearance of CA:OX peaks at 840, 895, 1319, and 1405  $\text{cm}^{-1}$  and disappearance of CA:MO peaks at 790, 905, 1330, and 1415  $\text{cm}^{-1}$ .

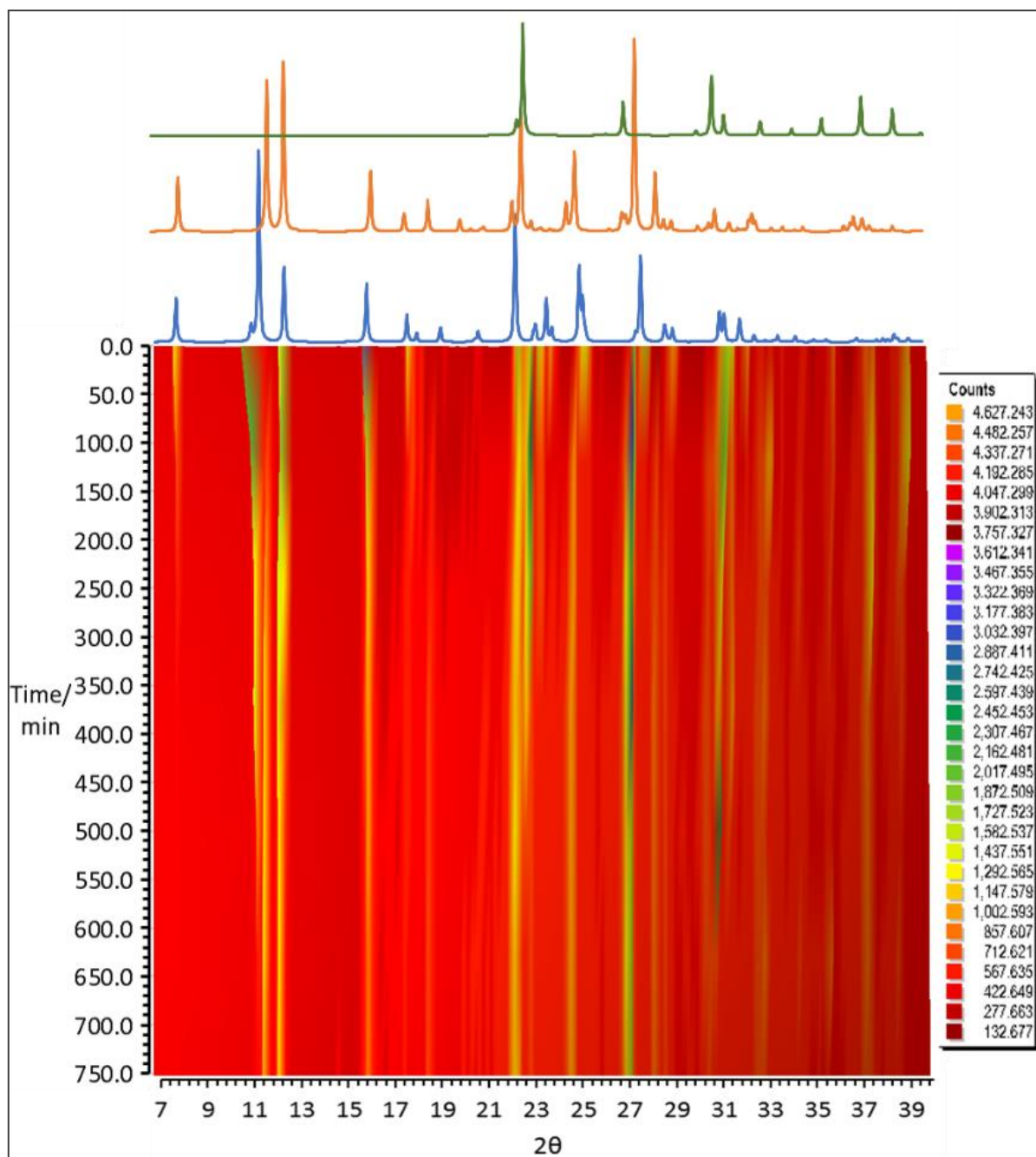


**Figure 7:** *In-situ* high temperature powder X-ray diffraction pattern of solvent free transformation of CA:MO to CA:OX in the presence of OX at isothermal conditions at 70 °C. Standard patterns are placed on the top: (Green) PXRd of OX, (Orange) CA:OX, and (Blue) CA:MO.

Kinetics show gradual decline in CA:MO fraction with simultaneous raise in CA:OX fraction and the extrapolation of kinetics from VT\_PXRd data is described in the SI. Kinetics at each isothermal condition (70, 80, 90, 100 °C) showed similar trends except that reaction rate increases as temperature increases. Moreover, the reaction was completed around 700, 90, 50, and 20 minutes for 70, 80, 90, and 100 °C, respectively (Figure 8).

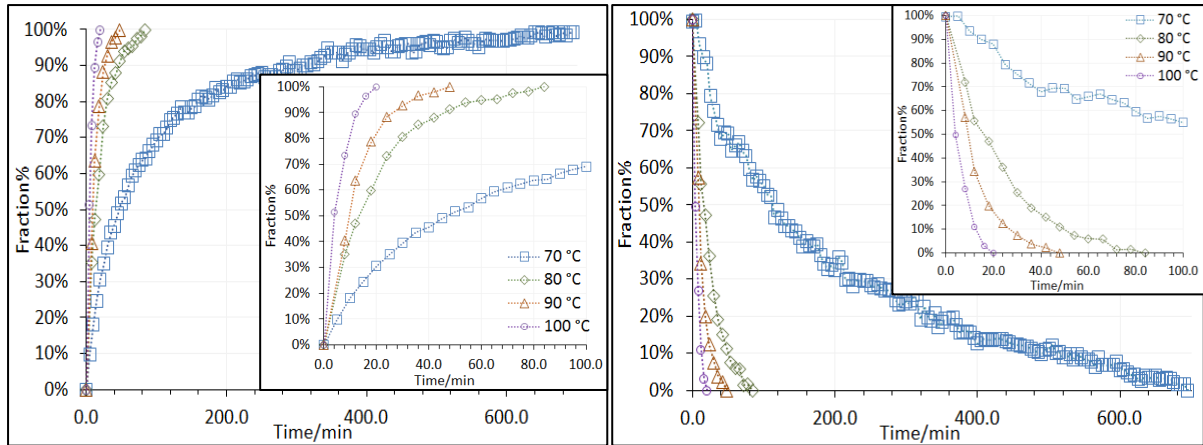


**Figure 8:** Kinetics of CA:OX growth (Left), and CA:MO dissolution (Right) at 65, 75, 90, and 100 °C.

Competitive destabilization can be kinetically described using potential energy diagram (Figure 9). As reaction progresses, the reactants constantly gain potential energy until reaching a transient high energy state. The amount of potential energy gained is equal to the activation energy ( $E_a$ ) of that reaction which is the minimum energy required for a system to initiate a given reaction.  $E_a$  (kJ/mol) is commonly calculated using Arrhenius equation (Equation 5), which is based on the proportionality between reaction rate constants and temperature. <sup>14</sup>

$$\ln k = \ln A - \frac{E_a}{RT} \dots \dots (Eq5)$$

Where  $k$  is the rate constant,  $A$  is a pre-exponential factor and it reflects the molecular collision frequency required for the reaction.

The high-energy state then rearranges itself to form the thermodynamically more stable phase at a given temperature and pressure. The difference between potential energy levels of the initial and final state is equal to the difference in lattice energies or Gibbs free energies between reactants and products. Both transient phase and activation energy are crucial parameters that allow to understand the reaction kinetics.

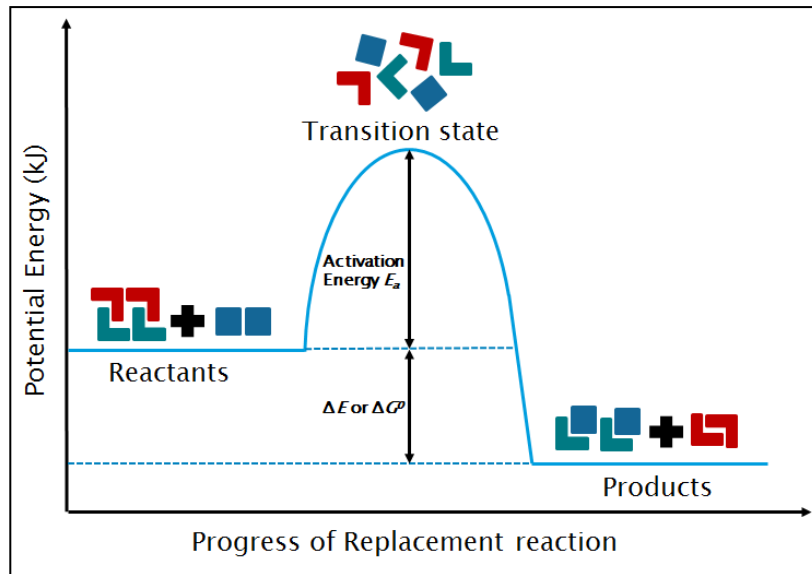


**Figure 9.** Thermodynamic ( $\Delta E$  and  $\Delta G^0$ ) and kinetic ( $E_a$ ) parameters used to describe the competitive destabilization reaction.

Mathematical treatment of these kinetics is primarily used to interpret the progress of a given reaction. Therefore, fraction change of a solid, or  $d(\alpha)$ , during a reaction is considered as a main variable, where  $\alpha$  is the conversion fraction and is a ratio of reacted solid amount over the total solid amount (Equation 6). The conversion can be expressed as a function of time, temperature, pressure, or composition.

$$\alpha(t) = \frac{A(t_0) - A(t)}{A(t_0)} \dots\dots (Eq6)$$

Where  $A(t_0)$  is the reactant amount at zero-time (total amount) and  $A(t)$  is the reactant amount at  $(t)$  time.

Mathematical treatment helps to describe experimental conversion values and to suggest a theoretical kinetic model and hence a reaction mechanism. Based on the suggested reaction mechanism, the models are classified as nucleation and growth controlled, geometrical contractions, diffusion, or reaction order models (Table 4).<sup>15</sup>

**Table 4:** Models used in fitting experimental kinetics of cocrystal transformations:

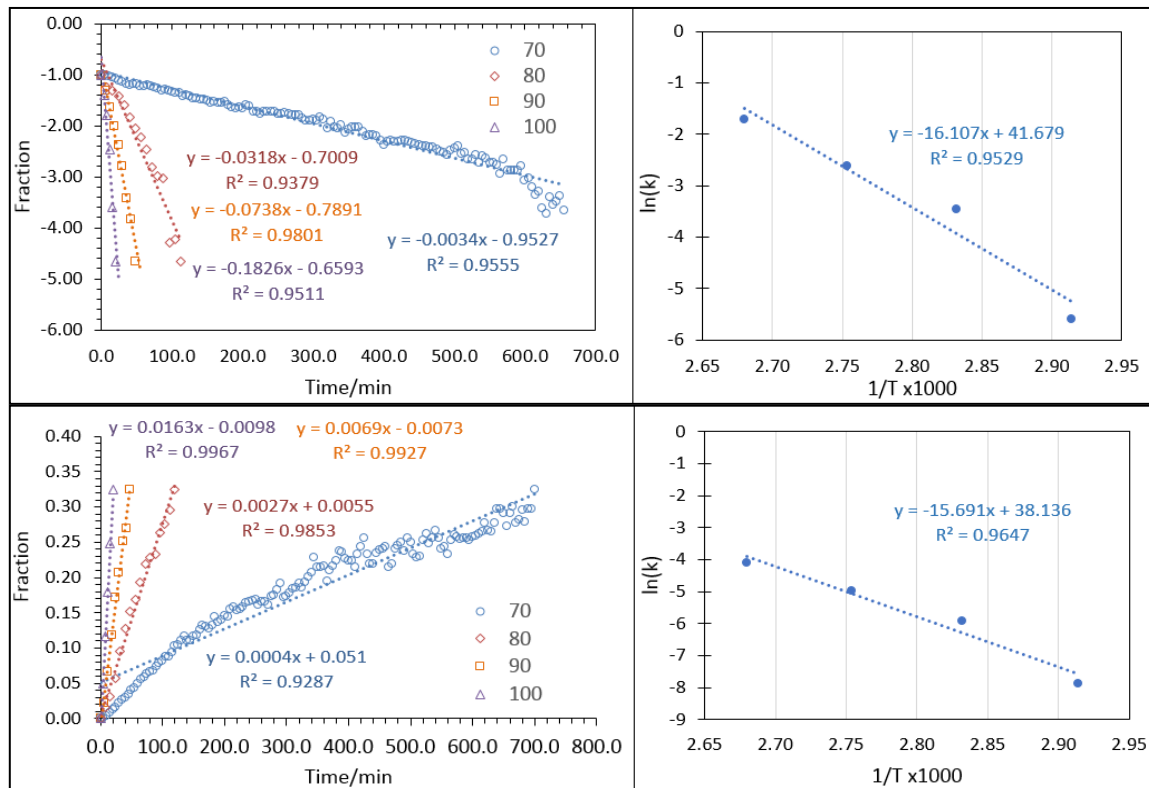
Kinetic Model	Abbreviation	Integral Function $g(\alpha)$
Nucleation and crystal growth models		
Prout - Tompkins	PT	$\ln [\alpha/(1 - \alpha)] = kt$
Avrami-Erofeev (n=2)	AE 2	$[- \ln (1 - \alpha)]^{1/2} = kt$
Avrami-Erofeev (n=3)	AE 3	$[- \ln (1 - \alpha)]^{1/3} = kt$
Reaction order models		
First order	FO	$[- \ln (1 - \alpha)] = kt$
Geometrical contraction models		
One-dimensional phase boundary	1D PB	$1 - \alpha = kt$
Two-dimensional phase boundary	2D PB	$1 - (1 - \alpha)^{1/2} = kt$
Three-dimensional phase boundary	3D PB	$1 - (1 - \alpha)^{1/3} = kt$
Diffusion models		
One dimensional diffusion	1D D	$\alpha^2 = kt$
Two-dimensional diffusion	2D D	$(1 - \alpha) \ln(1 - \alpha) + \alpha = kt$
Three-dimensional diffusion	3D D	$[1 - (1 - \alpha)^{1/3}]^2 = kt$
Ginstling-Brounshtein	GB	$1 - (2\alpha/3) - (1 - \alpha)^{2/3} = kt$

CA:MO destabilization and CA:OX formation curves were subjected to model fitting and  $r^2$  values were compared (Table 5). According to  $r^2$  values, CA:MO destabilization curves follow Prout-Tompkins model whereas CA:OX formation curves generally show higher  $r^2$  values and follow Ginstling – Brounshtien and 3D diffusion models.

The best models were then subjected to Arrhenius plotting (Figure 10) and activation energy ( $E_a$ ) was calculated accordingly. Best model for CA:MO destabilization was found to be Prout Tompkins with  $E_a$  of 133.91 kJ/mol. For CA:OX growth the best model in general was found to be Ginstling – Brounshtein diffusion with more inclination toward 3-dimensional diffusion model at 70 and 80 °C and thus  $E_a$  ranged from 130.45 - 132.57 kJ/mol. Moreover, destabilization rates of CA:MO were found higher (-0.00340 - -0.18263 min<sup>-1</sup>) compared to growth rates of CA:OX (0.00041 - 0.01630 min<sup>-1</sup>) (Table 6).

Prout – Tompkins is a nucleation and crystal growth-controlled model. This model applies when the reaction rate (destabilization rate in this case) is dependent on both the reacted ( $\alpha$ ) and unreacted amounts ( $1 - \alpha$ ) at each time interval. This type of reaction is called autocatalytic

where the reaction product can stimulate the progression of the reaction by formation of defects within crystal structure<sup>16</sup>. Prout-Tompkins model was observed to best describe kinetics of thermal decomposition reactions, such as  $\text{KMnO}_4$ .<sup>17</sup> Ginstling-Brounshtein model or 4D



diffusion is similar to 3D diffusion model but with the addition of Fick's first law of radial diffusion which assumes that reaction at interface is faster than diffusion.<sup>18</sup>

**Figure 10:** Isothermal kinetics, and Arrhenius plot of CA:MO destabilization (Up) following Prout-Tompkins and CA:OX growth (Down) following Ginstling – Brounshtien at 70, 80, 90, and 100 °C.

**Table 5:** Comparison of Model Fitting Correlation Coefficient Values ( $r^2$ ) of CA:MO Transformation Kinetics. Values in Red Indicate Highest Top Two  $r^2$  for Destabilization and Growth:

Model	CA:MO destabilization				CA:OX growth			
	70°C	80°C	90°C	100C	70°C	80°C	90°C	100
PT	<b>0.919</b>	<b>0.924</b>	<b>0.980</b>	<b>0.951</b>	0.217	0.321	0.852	0.908
AE n=2	0.729	0.612	0.609	0.699	0.893	0.934	0.928	0.959
AE n=3	0.841	0.760	0.732	0.804	0.838	0.859	0.871	0.924
1st order	0.370	0.324	0.397	0.512	0.954	0.980	0.875	0.865
1D PP	<b>0.841</b>	<b>0.817</b>	<b>0.765</b>	<b>0.841</b>	0.633	0.757	0.721	0.801

2D PP	0.691	0.617	0.598	0.689	0.843	0.921	0.927	0.966
3D PP	0.606	0.516	0.527	0.625	0.901	0.970	0.969	0.989
1D D	0.570	0.539	0.527	0.623	0.773	0.888	0.893	0.941
2D D	0.449	0.412	0.444	0.548	0.882	0.958	<b>0.974</b>	<b>0.994</b>
3D D	0.242	0.262	0.350	0.468	<b>0.966</b>	<b>0.988</b>	0.934	0.904
GB	0.380	0.352	0.406	0.516	<b>0.929</b>	<b>0.985</b>	<b>0.993</b>	<b>0.997</b>

**Table 6:** Summary of Kinetic Parameters Including Activation Energies ( $E_a$ ) for CA:MO Destabilization, and CA:OX Growth:

Temp	CA:MO destabilization			CA:OX growth		
	Model	Rate-min <sup>-1</sup>	$E_a$ kJ/mol	Model	Rate-min <sup>-1</sup>	$E_a$ kJ/mol
70 °C	PT	-0.00340	133.91	GB & 3DD	0.00041	132.57 - 130.45
80 °C	PT	-0.03175		GB & 3D D	0.00270	
90 °C	PT	-0.07383		GB	0.00694	
100 °C	PT	-0.18263		GB	0.01630	

## CONCLUSION:

The combination of thermal analysis, VT-PXRD, and sublimation experiments confirm the competitive destabilization of CA:MO by OX to form CA:OX. This process takes place only via vapor phase. No eutectic formation was observed in Raman spectroscopy, XRD, or HSM experiments where the destabilization reaction was completed before reaching the melting point of CA:MO cocrystal (132.1°C).  $\Delta E_{des}$ ,  $\Delta H_{fus-des}$  and  $\Delta G_{sub-des}$  values show that CA:OX formation is thermodynamically favorable. Both  $\Delta E_{des}$  and  $\Delta H_{fus-des}$  reflected that the cohesiveness of CA:OX cocrystal is greater compared to CA:MO. Whereas,  $\Delta G_{sub-des}$  data show that NG or heating of CA:MO + OX can generate sufficient vapor pressure to achieve destabilization of CA:MO. Additionally, the produced vapor pressure is at a supersaturation state with respect to CA:OX cocrystal, leading to its nucleation and crystal growth. Compared to previously reported CZ:NT and CZ:SA systems<sup>9</sup>, CA cocrystals display a different destabilization behavior where both lattice energies and vapor pressure related values contributed to the preference of CA:OX formation. Kinetic investigations show that CA:MO destabilization follows Prout – Tompkins model which is nucleation and crystal growth rate dependent with activation energy ( $E_a$ ) of 133.91 kJ/mol. Whereas, CA:OX formation is

diffusion rate dependent and mainly following Ginstling-Brounshtein model with  $E_a$  of 132.57 - 130.45 kJ/mol.

### **Supporting Information**

Supporting information is available as a separate PDF containing description of the experimental methods and supporting results. The supporting results involve DSC and TGA thermograms, PXRD patterns and Raman spectra of sublimation results, and *in-situ* VT\_PXRD patterns.

### **Corresponding Author**

Anant Paradkar, [a.paradkar1@bradford.ac.uk](mailto:a.paradkar1@bradford.ac.uk) and MHD. Bashir Alsirawan [m.b.alsirawan@bradford.ac.uk](mailto:m.b.alsirawan@bradford.ac.uk). Centre for Pharmaceutical Engineering Science, University of Bradford, Bradford, D7 1DP, United Kingdom.

### **Author Contributions**

The manuscript was written through contributions of all authors. All authors have given approval to the final version of the manuscript.

### **ACKNOWLEDGMENT**

Authors would like to thank EPSRC (EP/J003360/1, EP/L027011/1). M. Bashir would like to thank CARA for providing doctoral degree scholarship.

### **REFERENCES**

- (1) Rein, A. J.; Donahue, S. M.; Pavlosky, M. A. In Situ FTIR Reaction Analysis of Pharmaceutical-Related Chemistry and Processes. *Curr. Opin. Drug Discov. Devel.* **2000**, *3*, 734–742.
- (2) Sokolov, A. N.; Friscić, T.; MacGillivray, L. R. Enforced Face-to-Face Stacking of Organic Semiconductor Building Blocks within Hydrogen-Bonded Molecular Cocrystals. *J. Am. Chem. Soc.* **2006**, *128*, 2806–2807.

<https://doi.org/10.1021/ja057939a>.

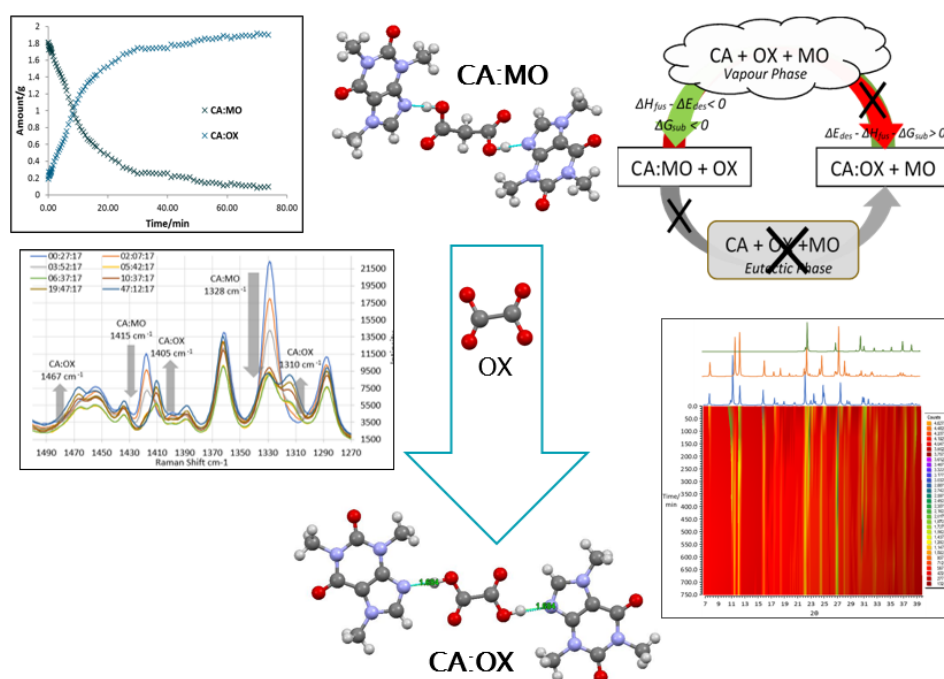
- (3) Braga, D.; Grepioni, F.; Shemchuk, O. Organic–Inorganic Ionic Co-Crystals: A New Class of Multipurpose Compounds. *CrystEngComm* **2018**, *20*, 2212–2220.  
<https://doi.org/10.1039/C8CE00304A>.
- (4) Spitzer, D.; Risse, B.; Schnell, F.; Pichot, V.; Klaumunzer, M.; Schaefer, M. R. Continuous Engineering of Nano-Cocrystals for Medical and Energetic Applications. *Sci. Rep.* **2014**, *4*. <https://doi.org/10.1038/srep06575>.
- (5) Qiao, N.; Li, M.; Schlindwein, W.; Malek, N.; Davies, A.; Trappitt, G. Pharmaceutical Cocrystals: An Overview. *Int. J. Pharm.* **2011**, *419*, 1–11.  
<https://doi.org/http://dx.doi.org/10.1016/j.ijpharm.2011.07.037>.
- (6) Good, D.; Miranda, C.; Rodríguez-Hornedo, N. Dependence of Cocrystal Formation and Thermodynamic Stability on Moisture Sorption by Amorphous Polymer. *CrystEngComm* **2011**, *13*, 1181–1189. <https://doi.org/10.1039/C0CE00592D>.
- (7) Fischer, F.; Lubjuhn, D.; Greiser, S.; Rademann, K.; Emmerling, F. Supply and Demand in the Ball Mill: Competitive Cocrystal Reactions. *Cryst. Growth Des.* **2016**, *16*, 5843–5851. <https://doi.org/10.1021/acs.cgd.6b00928>.
- (8) Alsirawan, M. B.; Vangala, V. R. V. R.; Kendrick, J.; Leusen, F. J. F. J. J.; Paradkar, A. Coformer Replacement as an Indicator for Thermodynamic Instability of Cocrystals: Competitive Transformation of Caffeine:Dicarboxylic Acid. *Cryst. Growth Des.* **2016**, *16*, 3072–3075. <https://doi.org/10.1021/acs.cgd.6b00458>.
- (9) Alsirawan, M. B.; Lai, X.; Prohens, R.; R Vangala, V.; Shelley, P.; J Bannan, T.; O. Topping, D.; Paradkar, A. Mechanistic Understanding of Competitive Destabilization of Carbamazepine Cocrystals under Solvent Free Conditions. *Cryst. Growth & Des.* **2020**, *0*. <https://doi.org/10.1021/acs.cgd.0c00735>.
- (10) Titapiwatanakun, V.; Basit, A. W.; Gaisford, S. A New Method for Producing Pharmaceutical Co-Crystals: Laser Irradiation of Powder Blends. *Cryst. Growth Des.* **2016**, *16*, 3307–3312. <https://doi.org/10.1021/acs.cgd.6b00289>.
- (11) Lehmann, C. W.; Stowasser, F. The Crystal Structure of Anhydrous  $\beta$ -Caffeine as Determined from X-Ray Powder-Diffraction Data. *Chem. - A Eur. J.* **2007**, *13*, 2908–

2911. <https://doi.org/10.1002/chem.200600973>.
- (12) Cesaro, A.; Starec, G. Thermodynamic Properties of Caffeine Crystal Forms. *J. Phys. Chem.* **1980**, *84*, 1345–1346. <https://doi.org/10.1021/j100448a011>.
- (13) Booth, A. M.; Markus, T.; Mcfiggans, G.; Percival, C. J.; McGillen, M. R.; Topping, D. O. Design and Construction of a Simple Knudsen Effusion Mass Spectrometer (KEMS) System for Vapour Pressure Measurements of Low Volatility Organics. *Atmos. Meas. Tech* **2009**, *2*, 355–361. <https://doi.org/10.5194/amt-2-355-2009>.
- (14) Arrhenius Svante. Über Die Dissociationswärme Und Den Einfluss Der Temperatur Auf Den Dissociationsgrad Der Elektrolyte. *Zeitschrift für Physikalische Chemie*. 1889, p 96. <https://doi.org/10.1515/zpch-1889-0408>.
- (15) Khawam, A.; Flanagan, D. R. Solid-State Kinetic Models: Basics and Mathematical Fundamentals. *J. Phys. Chem. B* **2006**, *110*, 17315–17328. <https://doi.org/10.1021/jp062746a>.
- (16) Brown, M. E. The Prout-Tompkins Rate Equation in Solid-State Kinetics. *Thermochim. Acta* **1997**, *300*, 93–106. [https://doi.org/10.1016/S0040-6031\(96\)03119-X](https://doi.org/10.1016/S0040-6031(96)03119-X).
- (17) Prout, E. G.; Tompkins, F. C. The Thermal Decomposition of Potassium Permanganate. *Trans. Faraday Soc.* **1944**, *40*, 488. <https://doi.org/10.1039/tf94444000488>.
- (18) Wyandt, C. M.; Flanagan, D. R. Solid-State Non-Isothermal Kinetics of Sulfonamide-Ammonia Adduct Desolvation. *Thermochim. Acta* **1992**, *196*, 379–389. [https://doi.org/10.1016/0040-6031\(92\)80101-2](https://doi.org/10.1016/0040-6031(92)80101-2).

For Table of Contents Use Only and Synopsis

# Solid-State Competitive Destabilization of Caffeine Malonic Acid Cocrystal: Mechanistic and Kinetic Investigations

MHD. Bashir Alsirawan,<sup>a</sup> Xiaojun Lai,<sup>b</sup> Rafel Prohens,<sup>c</sup> Venu R. Vangala,<sup>a</sup> Petroc Shelley,<sup>d</sup> Thomas J. Bannan,<sup>e</sup> David O. Topping,<sup>d,e</sup> and Anant Paradkar<sup>\*a</sup>



Stability of cocrystals in multicomponent systems is a major subject and require comprehensive understanding of interactions between cocrystals and the other additives. Competitive destabilization of cocrystals occurs if structurally similar additive is present. Competitive destabilization caffeine : malonic acid cocrystal in presence of oxalic acid at solvent free

conditions is mediated by vapor phase formation. Kinetic studies revealed reaction rate dependency on nucleation-crystal growth and diffusion models for caffeine : malonic acid destabilization and caffeine : oxalic acid formation, respectively.